Finding SEIS North on Mars: Comparisons between SEIS sundial, Inertial and Imaging measurements and consequences for seismic analysis

D. Savoie[a,b,*], A. Richard[b,**], M. Goutaudier[b], P. Lognonné[c], K. Hurst[d], J.N. Maki[d], M. Golombek[d], M. Van Driel[e], J. Clinton[e], E. Stutzmann[c], D. Mimoun[f], W.B. Banerdt[d], N. Williams[d]

[a]*SYRTE, Observatoire de Paris, Université PSL, CNRS, Sorbonne Université, LNE, 61 avenue de l'Observatoire 75014 Paris, France*
[b]*Palais de la Découverte, Av. Franklin D. Roosevelt, 75008 Paris, France*
[c]*Université de Paris, Institut de Physique du globe de Paris, Paris, F75005, France*
[d]*NASA Jet Propulsion Laboratory, Pasadena, California Institute of Technology*
[e]*Institute of Geophysics, ETH Zurich, Zurich, Switzerland.*
[f]*Institut Supérieur de l'Aéronautique et de l'Espace, ISAE, Toulouse, France*

Abstract

In this paper, we present the results obtained in the determination of the true North direction on Mars by using a gnomon on the InSight mission and compare the measurements with either the North determination from the Inertial Measurement Unit and Imaging analysis. The obtained measurement has been use to populate the SEIS orientation information in the archived SEIS data. Images taken during December 2018 and January 2019 allows to determine the gnomon shadow position and length over a target. By calculating the Sun local coordinates using planetary ephemeris VSOP87, the images are used to estimate the true North direction on the landing site. By using eight different images, we obtain the true North direction with an accuracy up to 2.5°, which is confirmed by the IMU and Imaging analysis. The true North direction is also confirmed by an image taken near local noon, when the sun crosses the meridian. The North determination precision is then discussed in view of the seismic determination of the back-azimuth.

NASA's InSight landing on Mars took place on November 26, 2018. After a few weeks of surface operations, InSight deployed the seismometer package SEIS (Seismic Experience for Interior Structure) (Lognonné et al., 2019) on the martian surface and provided first results (Banerdt et al., 2020; Giardini et al., 2020; Lognonné et al., 2020). Many of the SEIS scientific investigations were made by the 3 axis capability of the SEIS instrument, enabling the measurement, in the North, East, vertical local reference, of the ground acceleration. This paper is therefore focused on the methods used to determine this reference frame. While SEIS has its vertical axis, thanks to its Leveling system, aligned with the local gravity to within less than 0.1° , the determination of its azimuth with respect to North was more difficult.

*Corresponding author
**Principal corresponding author
Email addresses: denis.savoie@obspm.fr (D. Savoie), andy.richard@universcience.fr (A. Richard), marc.goutaudier@universcience.fr (M. Goutaudier)

The top of the instrument is equipped with a handle used during deployment that also doubles as a gnomon. A gnomon is the main tool of a sundial: a vertical stick projecting a shadow on a target. It enables, by its shadow, the determination of the Sun's position in the sky, and thus by extension in our case the seismometer's position and orientation on the Martian surface. For Insight, the technique did not necessitated any active sensor, as it used in an opportunistic way the InSight camera Maki et al. (2018) and the deployment handle. This was simpler than the north sensor of the Small Surface Stations of Mars 96 (Linkin et al. (1998)) (unfortunately lost after launch in 11/1996), which had also to determine the North for the magnetic components of the OPTIMISM experiment (Kuhnke et al. (1998); Lognonné et al. (1998)). Their North sensor, mounted on the deployed magnetometer, was monitoring the light intensity through a small hole with a known direction with respect to the 3 axis of the magnetometer.

The gnomon was only visible for a few days after the deployment of SEIS, the seismometer was subsequently covered by the Wind and Thermal Shield (WTS) before starting its operation phase. The process to determine the true North direction by using a gnomon on Mars was described by Savoie et al. (2019), from which this paper is the conclusion.

In this paper, we describe the procedures and results obtained during the few days after the SEIS seismometer was deployed on the martian surface, in order to determine the North with the gnomon. We first describe the method used to analyze the InSight camera images. Determination of the true North requires to be able to identify the whole shadow on low quality images deformed by the perspective. Then, we describe the results obtained for the true North direction on the different images.

We then compare the gnomon North determination with an independent measure of the lander azimuth, as obtained from the Inertial Measurement Unit. From that azimuth and the exact knowledge of the Instrument Deployment Arm imager, it was therefore possible to determine also the direction of North with respect to SEIS. A second comparison is then done through the analysis of remote sensing data and their comparison with the lander panorama images.

We conclude the paper by comparing the orientation errors with the back-azimuth determination of seismic signals and confirm that the North orientation is meeting all the seismological needs. The SEIS orientation presented in this paper has been used as reference, and is included in the SEIS metadata InSight Mars SEIS Data Service (2019).

1. Images taken by the Instrument Deployment Camera (IDC)

After landing, images of the sundial were acquired by the Instrument Deployment Camera (IDC), described by Maki et al. (2018). The IDC has an angular resolution of approximately 0.82 milli-radians/pixel at the center of the image and a field of view of 45 degrees (horizontal) x 45 degrees (vertical). After the deployment of SEIS on the surface on December 19, 2018, IDC images of the sundial were acquired with the camera located on the robotic arm at approximately 1 meter above the sundial.

1.1. Images source

The images are published on the InSight mission website[1] and labelled with date and local mean solar time (LMST). The first images with a clearly visible shadow were taken on January

[1] `https://mars.nasa.gov/insight/multimedia/raw-images`

1st, 2019. To determine the true North direction, we used eight images acquired on January 1st, 2019, and labelled from 12h51m03s to 15h38m58s LMST (see for example Figure 1).

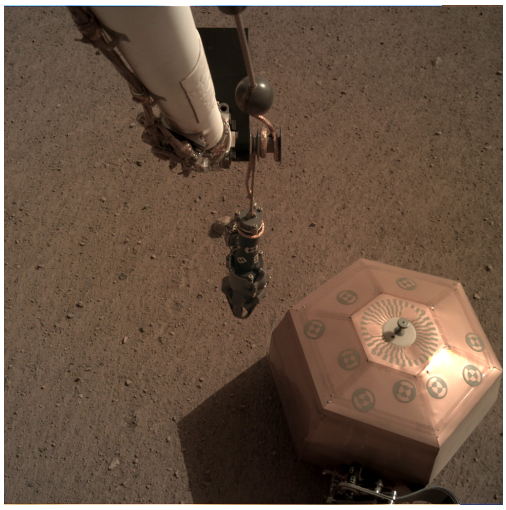

(a) 01/01/19 - 15h09m51s LMST

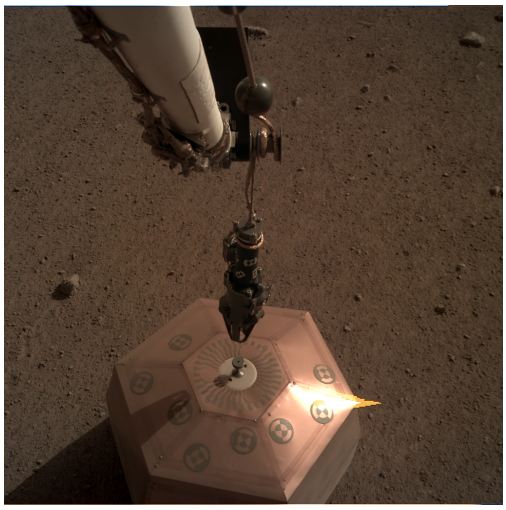

(b) 01/01/19 - 15h38m58s LMST

Figure 1: Images of the sundial taken on January 1st, 2019. The gnomon shadow is visible, on the target that is used to measure the azimuth of the Sun.

Due to a very tight schedule for the InSight ground operations, these images were taken within a few minutes range, thus having very similar shadow positions and lengths. As explained by Savoie et al. (2019), this configuration is not ideal to reach the accuracy of 1° in true North direction but it allows to reach the expected accuracy of 5° nonetheless.

Furthermore, the image taken near local noon can be used as a confirmation of the true North direction estimation, the Sun being close to the meridian. On this particular image however, the Sun is passing high in the sky and the gnomon shadow is too short to reach the target on the sundial. Its direction can still be used to confirm the results obtained with images taken in the afternoon.

In this study, we neglected the non-horizontality of the sundial which was measured as below 0.1° after the deployment phase of SEIS.

1.2. Determination of the time

The images file names contain the spacecraft clock time given in seconds elapsed since J2000 (see Fig. 2). This timing is given by the free-running onboard clock, and is thus not synchronized with UTC since the spacecraft launch. Since May 2018, the onboard clock has regularly drifted, and continued to do so after landing as seen on Figure 3. This drift is caused by an expected error on the crystal oscillator frequency of the onboard clock. The conversion from spacecraft time to UTC can be made by using the WebGeocalc algorithm[2]. For example, the first image taken on January 1st, 2019 (Sol 35) contain a timestamp of 599635689 seconds after J2000. This timestamp

[2] `https://wgc.jpl.nasa.gov:8443/webgeocalc/#TimeConversion`

corresponds to January 1st, 2019 at 17h28m38s UTC. By using our algorithm (Savoie et al., 2019), this time is converted to 12h49m37s LMST on InSight landing site.

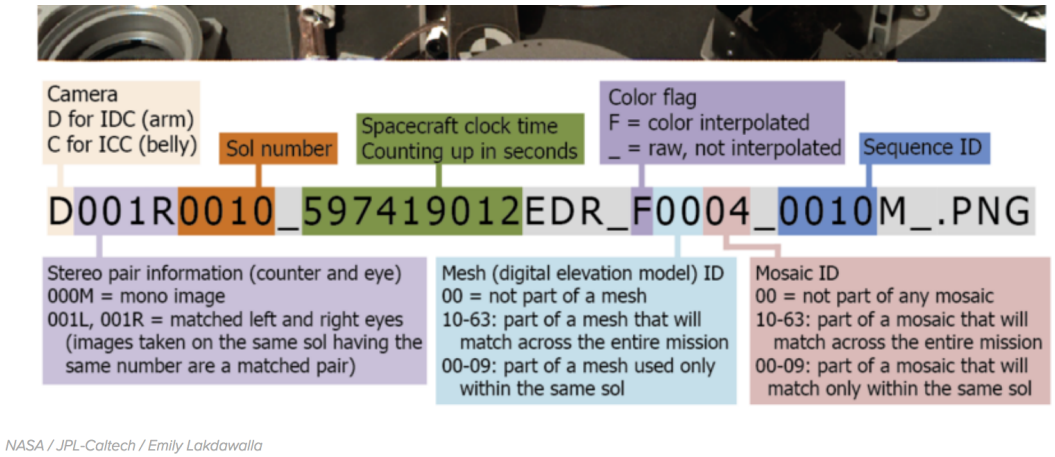

Figure 2: Description of the information contained in the image file name.

It is important to notice that this local mean solar time value is different from the one published on the JPL website. For this particular image, the description reads 12h51m02s LMST, thus a time difference of 85 seconds with our calculation.

As detailed by Savoie et al. (2019), the Sun azimuth is off by $\pm 0°6'$, equivalent to an error of 10 seconds in timing. A difference of 85 seconds induces an azimuth error of maximum $54'$ for the date of January 1st 2019. This difference induced in the shadow position is below our reading accuracy on the sundial images. This time shift of 85 seconds can be imputed to the local time conversion algorithm used by JPL which uses optimal lander coordinates.

The local mean solar time conversion algorithm used by the JPL, implemented in NAIF/SPICE kernels[3] is based on the InSight target landing site coordinates 4.46°N and 135.97°E. However, those coordinates correspond to the optimal landing site, and are different from the real lander planetocentric coordinates which are 4.50247°N, 135.6180843°E (Parker et al., 2019).

The main difference between these two sets of coordinates is in the longitude. InSight landed about 0.35° (*i.e.* 20 km) west-northwest of the planned landing site. Due to Mars rotation, a difference of 0.35° of longitude for the landing site induces a time shift of about 84 seconds in local mean time.

The coordinates of InSight after landing were updated in the NAIF/SPICE Kernel in April 2019[4]. This difference does not have an impact on the other scientific activities of the InSight mission, however the sundial is sensitive to any error in position and/or timing.

The reader should also be aware that images taken before December 29th, 2019 are labelled on the JPL website with a wrong local mean solar time value. The value given is actually the local true solar time, which differs from the previous one by almost 50 minutes.

[3] `https://naif.jpl.nasa.gov/pub/naif/INSIGHT/kernels/sclk/insight_lmst_ops181206_v1.tsc`
[4] `https://naif.jpl.nasa.gov/pub/naif/INSIGHT/kernels/fk/insight_tp_ops181206_iau2000_v1.tf`

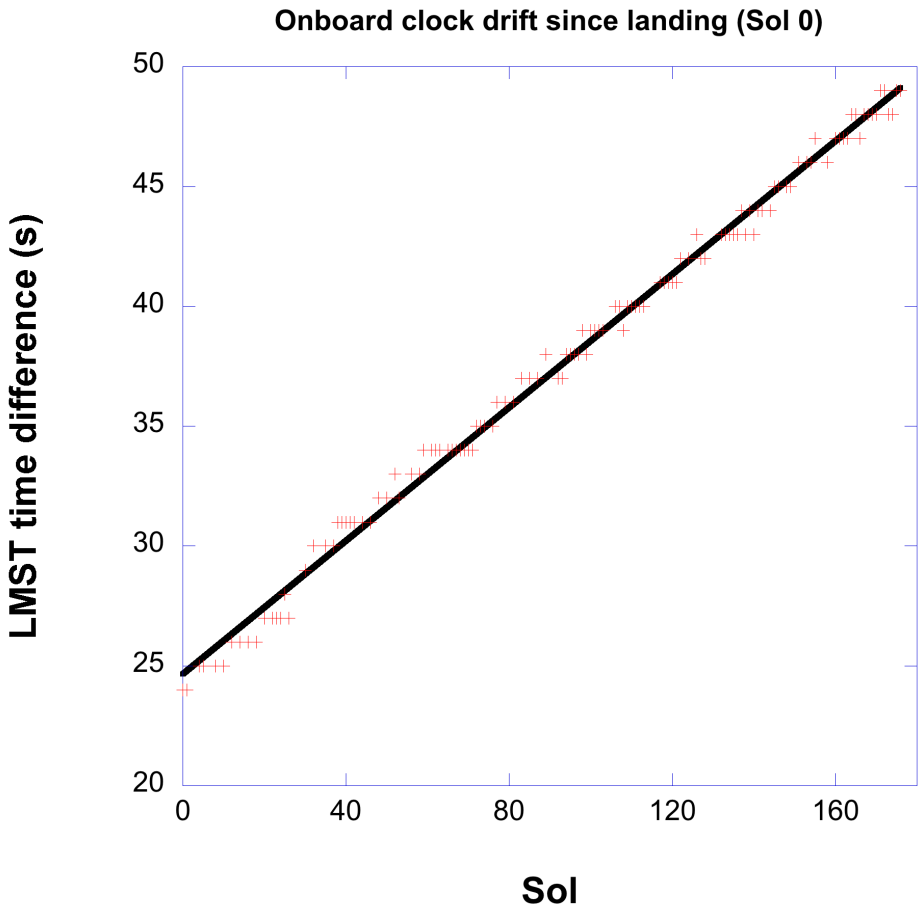

Figure 3: Drift in the Local Mean Solar Time due to the free-running onboard clock on InSight spacecraft. The data are plotted for 6 months from Sol 0 (Nov. 26th, 2018). The dark line is fitted on data, and corresponds to a linear increase of the drift of 0.139 seconds per sol.

2. True North direction on images

On the sundial, the shadow marks the opposite direction of the Sun. Thus, measuring the shadow position on the sundial at a precise UTC time value provides the Sun azimuth on the pictures. Computing the azimuth of the Sun on Mars allows to determine, on each picture, the location of the North-South axis from which it is measured.

2.1. Shadow direction

A precise determination of the shadow top and direction is difficult due to the odd shape and geometry of the gnomon (see Savoie et al. (2019) for a precise description). Due to the gnomon elevation compared to the target level, the center of the whole target has to be determined on each picture.

The target is divided in three concentric rings, each one of them divided into 72 segments of 5° each. The borders of opposite segments can be prolongated through the whole target plane in order to determine the target center.

The defined center can be used to trace rays fitting the round shadow borders. Then, the median provides the shadow direction (Figure 4).

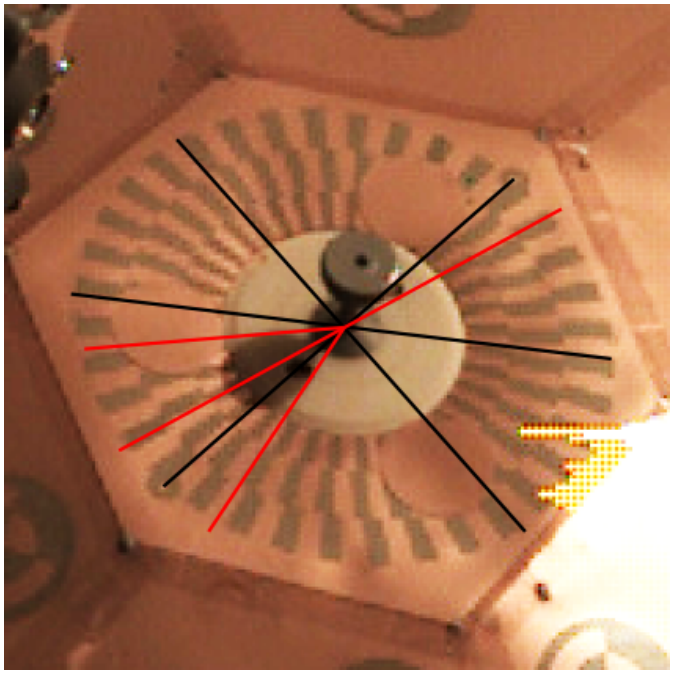

Figure 4: Estimation of the shadow direction on the image taken on 01/01/19 at 15h11m47s LMST. Dark rays defines the shadow center and red rays define the shadow border and shadow top direction.

2.2. Local Sun azimuth

The determination of the shadow direction provides the sun direction on the pictures. This direction can be computed by determining azimuth measured in the clockwise direction from the true South. For each picture, we computed the solar coordinates for a martian observer as described by Savoie et al. (2019). The azimuth and altitude values obtained for the images of January 1st, 2019 are provided in Table 1.

As expected for this local time, the altitude of the Sun is decreasing in the afternoon sky on InSight landing site. Also, its azimuth is increasing as the Sun is moving towards West ($A = 90°$).

2.3. True North direction results

On each image, we used the method described earlier to determine the top of the shadow, and thus the Sun direction. The azimuth of the Sun associated then leads to the North-South axis. The results are given here for two of the eight different images taken on January 1st, 2019 (Fig.5 and 6). Each image is compared with a simulation and labelled with time in UTC, Local Mean Solar Time (LMST), Local True Solar Time (LTST), angles H (hour angle), α (right ascension), δ (declination), A (azimuth) and h (altitude) expressed in degrees and the shadow length in millimeters.

2.4. Discussion

On the two images presented here, the True North direction is determined using the computed Sun azimuth. By using the gnomon shadow top, determined as precisely as possible considered the shape of the instrument and images resolution, the North-South axis is graphically determined. The axis is drawn as a black line on both pictures. A difference of almost half a segment on the

File name (sec since J2000)	**Time** UTC	LMST	LTST	**Azimuth** A (°)	**Altitude** h (°)
599635689	17:28:38	12:49:37	12:00:24	0.2589	68.4926
599644246	19:51:15	15:08:25	14:19:11	57.1352	49.4614
599644365	19:53:14	15:10:21	14:21:08	57.4756	49.0567
599645280	20:08:29	15:25:12	14:35:57	59.8710	45.8976
599645795	20:17:04	15:33:33	14:44:18	61.0645	44.0868
599645918	20:19:07	15:35:32	14:46:18	61.3348	43.6513
599646041	20:21:10	15:37:32	14:48:18	61.5996	43.2146
599646321	20:25:50	15:42:05	14:52:50	62.1830	42.2166

Table 1: Computed Sun local coordinates for InSight images on 01/01/2019.

target is visible between the two pictures. Since a segment has a thickness of 5°, the deviation between the two images correspond to almost 2.5°.

These two images corresponds to the maximum deviation we obtain on the eight images of January 1st. Based on those images, the True North direction on InSight landing site can be determined within a 2.5° range. Unfortunately, this result is over the expected 1° accuracy for an optimal martian sundial use. This lack of accuracy can be explained by the very similar shadow positions induced by images taken on a very short time range. The accuracy of this measurement could have been increased by images taken through the whole day, morning and afternoon, as suggested by Savoie et al. (2019).

However, an accuracy of 2.5° on the True North direction is below the required accuracy of 5° of the SEIS instrument. The sundial experiment thus match its requirements.

3. Location of SEIS and knowledge of North

The location of the InSight spacecraft on the surface of Mars has been determined in both inertial space by X-band radio tracking by the Rotation and Interior Structure Experiment (RISE) (Folkner et al., 2018) and by a high-resolution image acquired from orbit that clearly resolves the lander and the large circular solar panels that has been georeferenced to the cartographic grid (Golombek et al., 2020a). A 30 cm/pixel High-Resolution Imaging Science Experiment (HiRISE) image acquired on December 6, 2018 after landing has been carefully georeferenced to image and topographic basemaps composed of 12.5 m/pixel High-Resolution Stereo Camera (HRSC) images, 6 m/pixel MRO Context Camera (CTX) images in the International Astronomical Union/International Association of Geodesy, IAU/IAG 2000 positive East planetocentric coordinate system with 463 m/pixel Mars Orbiter Laser Altimeter (MOLA) elevation postings as its base. In this system, the center of the lander is located at 4.50238417°N, 135.62344690°E, at an elevation of −2613.426 m (Golombek et al., 2020a).

After placing SEIS in the workspace to the south of the lander, several methods were used to

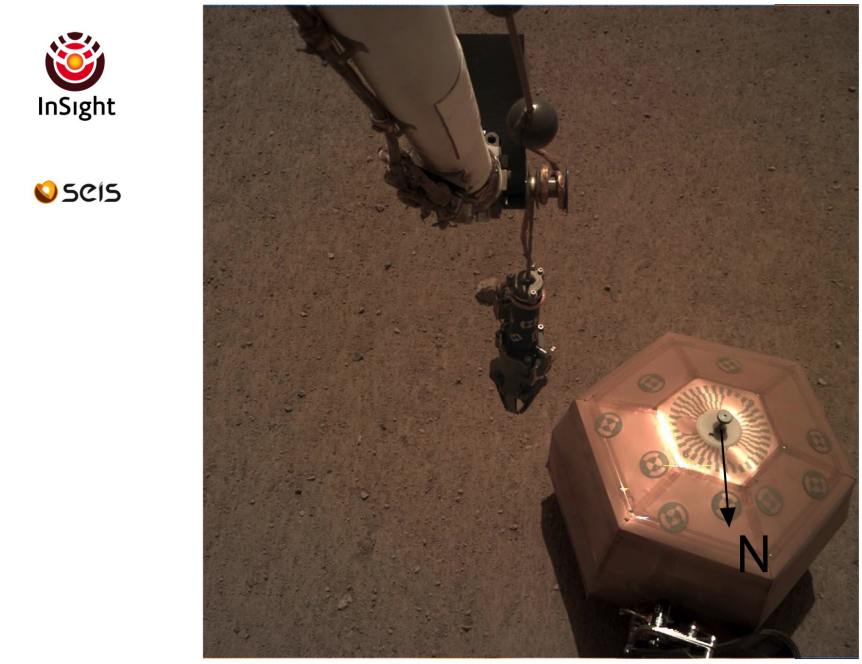

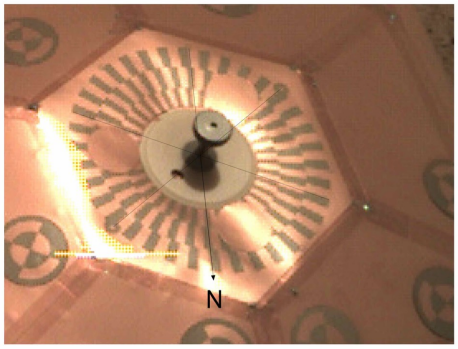

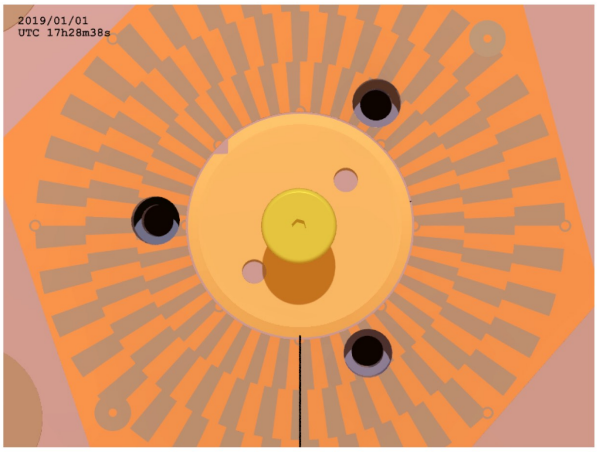

UTC = 17h28m38s
LMST = 12h49m37s
LTST= 12h00m24s
H = 0.0992°
α = 319.6436°
δ = -16.9434°
A = 0.2589°
h = 68.4926°
shadow =19.8 mm

sol 35 1/01/2019

Figure 5: True North direction for image taken on Sol 35 (1-1-2019), 17h28m38s UTC.

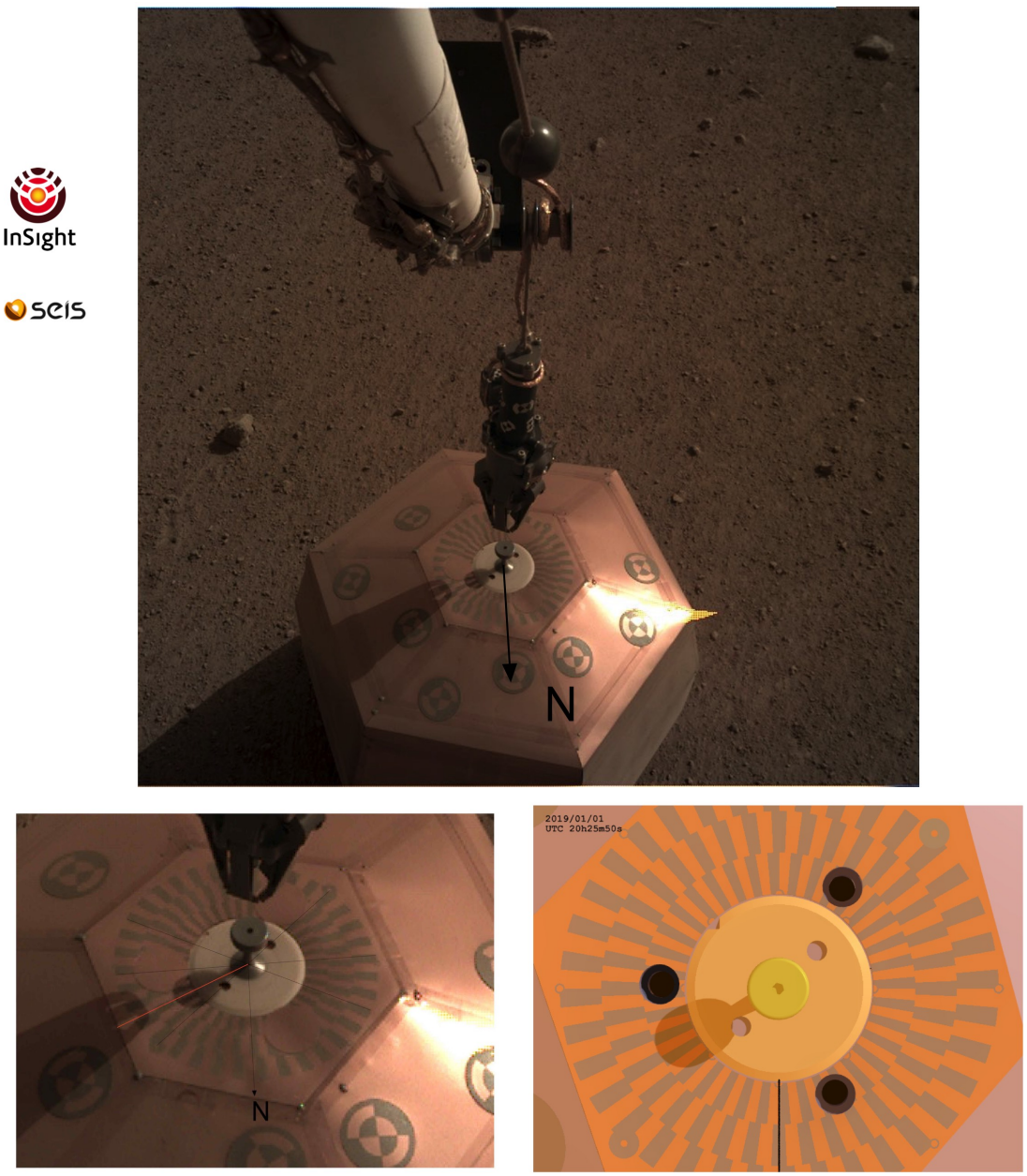

Figure 6: True North direction for image taken on Sol 35 (1-1-2019), 20h25m50s UTC.

determine its location (Golombek et al., 2020b). Stereo IDC images of the instruments and their fiducial points were used as was the physical location of the arm by moving the grapple (used to pick up the instruments) directly above it. These determinations were made in spacecraft centered coordinate systems. IDC stereo mosaics were also tied to the HiRISE image by transforming the spacecraft coordinate systems into the cartographic frame (Golombek et al., 2020b). These different methods locate the grapple/hook point of SEIS at 4.50234460°N, 135.62343703°E with its feet at an elevation of −2613.4 m with respect to the MOLA geoid.

The transformation of lander coordinates to Mars (the site frame) includes knowledge of the spacecraft yaw, pitch and roll recorded by the spacecraft Inertial Measurement Unit (IMU) (Golombek et al., 2020b). To test if there are any errors in our knowledge of the orientation of the spacecraft, the azimuths of features that are in view in both the surface panoramas and the HiRISE image were compared. The azimuths of around 35 features matches to within 1°. The best matched features greater than 50 m away, where discrepancies would be greatest, agree to an average of 0.5°. This suggests that the orientation (including the azimuth and tilt) recorded by the IMU and used to determine the site frame are accurate. This also means that analyses using lander images that depend on the location, azimuth and tilt of the spacecraft are accurate.

4. North determination with Intertial Measurement Unit and Robotic Arm imaging of SEIS

Golombek et al. (2020b) gives SEIS ground location expressed in the site frame. The site frame was determined by IMU measurement during descent, with Z axis along the gravity vector, X north and Y east. Knowing SEIS center location, we define SEIS reference direction as the middle of one of its hexagonal border (see Figure 7). Angles of the hexagon can be computed as reference points expressed in the site frame. Using these reference points leads to the reference direction azimuth expressed from North true direction.

The azimuth of SEIS reference direction expressed using the site frame coordinates is of about 192.5 degrees (±1°).

This azimuth is in good agreement with the north direction obtained using the gnomon as seen in Figure 7, with an error of about 2 degrees.

5. Seismic requirements and seismic errors in Quakes azimuth determination

The Marsquake Service Clinton et al. (2018) maintains a catalogue of marsquakes (InSight Marsquake Service (2020)) that includes phase identification and location information, when possible. By April 2019, only 3 events have been detected that include clearly identifiable polarised motions for first arriving phases (Giardini et al. (2020)). Figure 8 shows vertical component seismograms and horizontal particle motions from the VBB sensor for these 3 events. The P-picks are taken from InSight Marsquake Service (2020). The time windows selected for polarization analysis and the horizontal particle motion are indicated in the time series. The red line on the particle motion plots indicate the chosen azimuth, the shaded grey area indicates the estimated uncertainty. The 180° degree ambiguity can be resolved by considering the vertical component polarity as described by Böse et al. (2017). The raw seismograms were only multiplied by gain and filtered in the range indicated in table 2; azimuths and errors are estimated visually. These errors are found much larger than those associated to the specific method used. Lognonné et al. (2020) for example

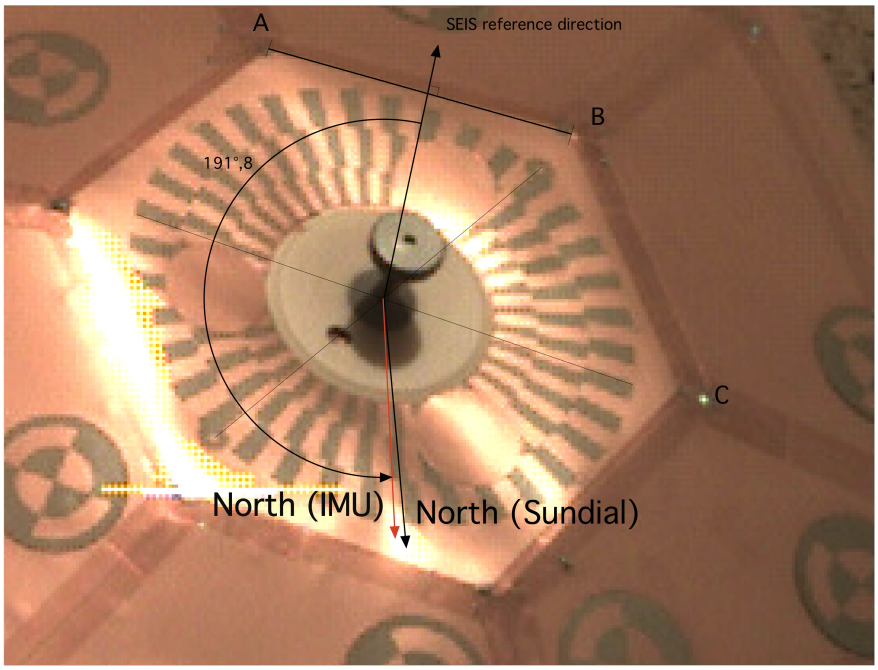

Figure 7: Comparison between sundial north determination and IMU north direction.

Table 2: Processing details for the azimuth determination in Fig 8.

event	filter range / Hz	window length / s	azimuth	error
S0173a	0.167 - 0.5	10	91°	±15°
S0235b	0.125 - 0.5	7	74°	±10°
S0183a	0.2 - 0.5	10	73°	±30°

used, for the event SO173, the polarization analysis of Schimmel et al. (2011) and found for the P an azimuth of 93° (larger by $2 \circ as the MQS one), while the azimuth of the S was ranging from 163.1°$ to 181° in the 03-0.4 Hz and 0.4-0.7 Hz bandwidth respectively. While the high frequency is found, as expected, almost orthogonal to the P one, the lower frequency illustrate the sensitivity of the techniques to both noise and, for the S wave, to the P seismic coda. In addition, lateral variation are expected to generate off-path perturbation of body waves as illustrated by several Earth studies (e.g. Otsuka (1966)).

6. Conclusion

By using eight images taken during Sol 35 of the InSight surface activity, we were able to estimate the Sun direction and compute its local coordinates over the landing site. The results presented in this paper show that we were able to graphically determine the True North direction on landing site within a 2.5° range. This accuracy is below the requirement of 5° for the SEIS experiment, and well below the level of uncertainty that can be estimated for marsquakes observed to date. Comparison of the north direction obtained with the gnomon measurements is compatible with IMU north direction of the lander within 2 degrees, comforting the use of such a simple device

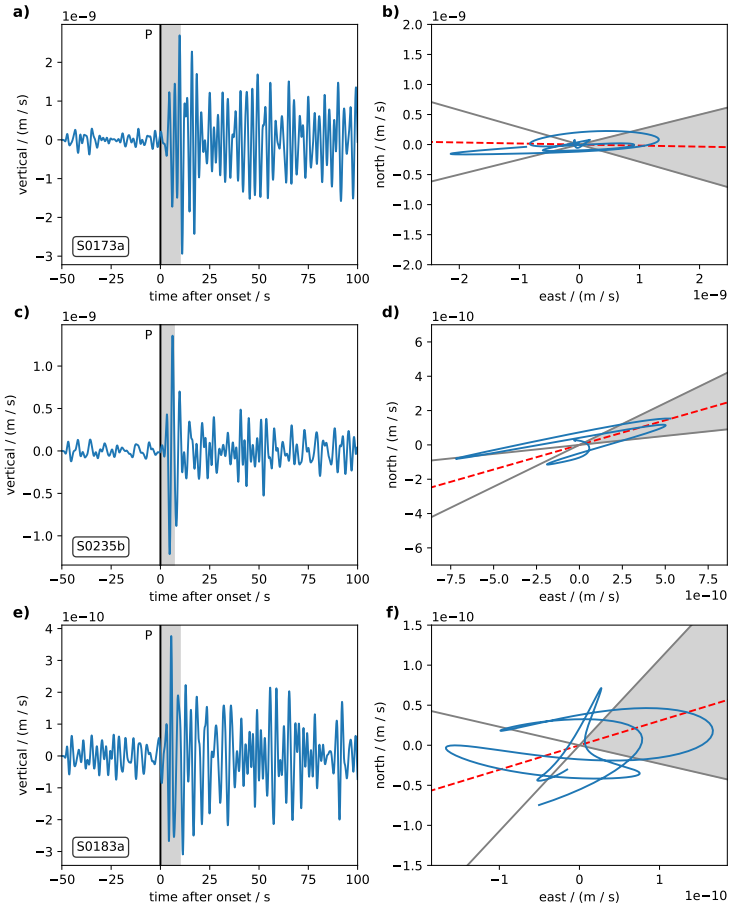

Figure 8: Vertical component VBB seismograms and horizontal particle motion for the three events with clearest polarization (S0173a, S0235b, S0183a). Details of the error estimates in the text.

as sundial for orientation of instruments on space missions.

In conclusion, the sundial did fulfill its expectations. It is a success for the first sundial on another planet, but we would like to inform the reader that the martian sundial is not the first extraterrestrial one. Most of the instruments installed on the Moon by Apollo missions as part of the Apollo Lunar Surface Experiments Package (ALSEP, see Sullivan (1994)), be it passive seismometers, laser reflectors (still used for Lunar laser ranging), the analyzer of ejecta and meteorites, *etc.*, were all oriented with the help of a gnomon whose shadow was projected on a target (fig. 9). In this case however, it is better to speak of "solar compass". Orientation on the Moon by the azimuth of the Sun was indeed extremely easy due to the very slow variation of this angle, which remains almost constant for several hours.

Figure 9: Gnomon used on the Moon with the passice seismic experiment (PSE) during the Apollo 14 mission.

The martian sundial experiment shows once again the possibilities of this ancient and passive tool for actual space missions.

Acknowledgments

All imaging data used in this paper are freely available at the Planetary Data system (PDS) at https://pds-imaging.jpl.nasa.gov/data/nsyt/insight_cameras/, including timing. SEIS data. We acknowledge NASA, CNES, their partner agencies and Institutions (UKSA, SSO, DLR, JPL, IPGP-CNRS, ETHZ, IC, MPS-MPG) and the flight operations team at JPL, SISMOC, MSDS, IRIS-DMC and PDS for providing SEED SEIS data used in section 5 and freely available at IPGP MSDS, IRIS-DMC and PDS (https://doi.org/10.18715/SEIS.INSIGHT.XB_2016).

The authors would like to thank Boris Semenov (JPL/NAIF Team) for its help on the time determination of SEIS images.

A portion of this work was supported by the InSight Project at the Jet Propulsion Laboratory, California Institute of Technology, under a contract with the National Aeronautics and Space Administration.

French co-authors acknowledge the support of CNES and of the Agence Nationale de la Recherche (ANR-14-CE36-0012-02 and ANR-19-CE31-0008-08).

This is InSight contribution number 175.

References

W. Bruce Banerdt, Suzanne E. Smrekar, Don Banfield, Domenico Giardini, Matthew Golombek, Catherine L. Johnson, Philippe Lognonné, Aymeric Spiga, Tilman Spohn, Clément Perrin, Simon C. Stähler, Daniele Antonangeli, Sami Asmar, Caroline Beghein, Neil Bowles, Ebru Bozdag, Peter Chi, Ulrich Christensen, John Clinton, Gareth S. Collins, Ingrid Daubar, Véronique Dehant, Mélanie Drilleau, Matthew Fillingim, William Folkner, Raphaël F. Garcia, Jim Garvin, John Grant, Matthias Grott, Jerzy Grygorczuk, Troy Hudson, Jessica C. E. Irving, Günter Kargl, Taichi Kawamura, Sharon Kedar, Scott King, Brigitte Knapmeyer-Endrun, Martin Knapmeyer, Mark Lemmon, Ralph Lorenz, Justin N. Maki, Ludovic Margerin, Scott M. McLennan, Chloe Michaut, David Mimoun, Anna Mittelholz, Antoine Mocquet, Paul Morgan, Nils T. Mueller, Naomi Murdoch, Seiichi Nagihara, Claire Newman, Francis Nimmo, Mark Panning, W. Thomas Pike, Ana-Catalina Plesa, Sébastien Rodriguez, Jose Antonio Rodriguez-Manfredi, Christopher T. Russell, Nicholas Schmerr, Matt Siegler, Sabine Stanley, Eléanore Stutzmann, Nicholas Teanby, Jeroen Tromp, Martin van Driel, Nicholas Warner, Renee Weber, and Mark Wieczorek. Initial results from the InSight mission on Mars. *Nature Geoscience*, February 2020. ISSN 1752-0894, 1752-0908. doi: 10.1038/s41561-020-0544-y.

M. Böse, J. F. Clinton, S. Ceylan, F. Euchner, M. van Driel, A. Khan, D. Giardini, P. Lognonné, and W. B. Banerdt. A probabilistic framework for single-station location of seismicity on Earth and Mars. *Physics of the Earth and Planetary Interiors*, 262:48–65, January 2017.

J. Clinton, D. Giardini, M. Böse, S. Ceylan, M. van Driel, F. Euchner, R. F. Garcia, S. Kedar, A. Khan, S. C. Stähler, B. Banerdt, P. Lognonne, E. Beucler, I. Daubar, M. Drilleau, M. Golombek, T. Kawamura, M. Knapmeyer, B. Knapmeyer-Endrun, D. Mimoun, A. Mocquet, M. Panning, C. Perrin, and N. A. Teanby. The Marsquake Service: Securing Daily Analysis of SEIS Data and Building the Martian Seismicity Catalogue for InSight. *Space Science Reviews*, 214(8):133, December 2018. ISSN 0038-6308, 1572-9672. doi: 10.1007/s11214-018-0567-5.

William M. Folkner, Véronique Dehant, Sébastien Le Maistre, Marie Yseboodt, Attilio Rivoldini, Tim Van Hoolst, Sami W. Asmar, and Matthew P. Golombek. The Rotation and Interior Structure Experiment on the InSight Mission to Mars. *Space Science Reviews*, 214(5), August 2018. ISSN 0038-6308, 1572-9672. doi: 10.1007/s11214-018-0530-5.

D. Giardini, P. Lognonné, W. B. Banerdt, W. T. Pike, U. Christensen, S. Ceylan, J. F. Clinton, M. van Driel, S. C. Stähler, M. Böse, R. F. Garcia, A. Khan, M. Panning, C. Perrin, D. Banfield, E. Beucler, C. Charalambous, F. Euchner, A. Horleston, A. Jacob, T. Kawamura, S. Kedar, G. Mainsant, J.-R. Scholz, S. E. Smrekar, A. Spiga, C. Agard, D. Antonangeli, S. Barkaoui, E. Barrett, P. Combes, V. Conejero, I. Daubar, M. Drilleau, C. Ferrier, T. Gabsi, T. Gudkova,

K. Hurst, F. Karakostas, S. King, M. Knapmeyer, B. Knapmeyer-Endrun, R. Llorca-Cejudo, A. Lucas, L. Luno, L. Margerin, J. B. McClean, D. Mimoun, N. Murdoch, F. Nimmo, M. Nonon, C. Pardo, A. Rivoldini, J. A. Rodriguez Manfredi, H. Samuel, M. Schimmel, A. E. Stott, E. Stutzmann, N. Teanby, T. Warren, R. C. Weber, M. Wieczorek, and C. Yana. The seismicity of Mars. *Nature Geoscience*, February 2020. ISSN 1752-0894, 1752-0908. doi: 10.1038/s41561-020-0539-8.

M. Golombek, N. H. Warner, J. A. Grant, E. Hauber, V. Ansan, C. M. Weitz, N. Williams, C. Charalambous, S. A. Wilson, A. DeMott, M. Kopp, H. Lethcoe-Wilson, L. Berger, R. Hausmann, E. Marteau, C. Vrettos, A. Trussell, W. Folkner, S. Le Maistre, N. Mueller, M. Grott, T. Spohn, S. Piqueux, E. Millour, F. Forget, I. Daubar, N. Murdoch, P. Lognonné, C. Perrin, S. Rodriguez, W. T. Pike, T. Parker, J. Maki, H. Abarca, R. Deen, J. Hall, P. Andres, N. Ruoff, F. Calef, S. Smrekar, M. M. Baker, M. Banks, A. Spiga, D. Banfield, J. Garvin, C. E. Newman, and W. B. Banerdt. Geology of the InSight landing site on Mars. *Nature Communications*, 11: 1014, February 2020a.

M. Golombek, N. Williams, N. H. Warner, T. Parker, M.G. Williams, I. Daubar, F. Calef, J. A. Grant, P. Bailey, H. Abarca, R. Deen, N. Ruoff, J. Maki, A. McEwen, N. Baugh, K. Block, L. Tamppar, J. Call, J. Ladewig, A. Stoltz, W.A. Weems, L. Mora-Sotomayor, and J. Torres. Location and setting of the InSight lander, instruments and landing site. *Earth ans Space Science*, submitted to InSight issue, May 2020b.

InSight Mars SEIS Data Service. Seis raw data, insight mission, 2019. URL `http://datacenter.ipgp.fr/networks/detail/XB_2016`.

InSight Marsquake Service. Mars seismic catalogue, insight mission; v2 2020-04-01, 2020. URL `http://www.insight.ethz.ch/seismicity/catalog/v2`.

Falko Kuhnke, Michel Menvielle, Günter Musmann, Jean Francois Karczewski, Holger Kügler, Claude Cavot, and Patrick Schibler. The OPTIMISM/MAG mars-96 experiment: magnetic measurements onboard landers and related magnetic cleanliness program. *Planetary and Space Science*, 46(6-7):749–767, June 1998. doi: 10.1016/s0032-0633(98)00010-5. URL `https://doi.org/10.1016/s0032-0633(98)00010-5`.

V. Linkin, A.-M. Harri, A. Lipatov, K. Belostotskaja, B. Derbunovich, A. Ekonomov, L. Khloustova, R. Kremnev, V. Makarov, B. Martinov, D. Nenarokov, M. Prostov, A. Pustovalov, G. Shustko, I. Järvinen, H. Kivilinna, S. Korpela, K. Kumpulainen, A. Lehto, R. Pellinen, R. Pirjola, P. Riihelä, A. Salminen, W. Schmidt, T. Siili, J. Blamont, T. Carpentier, A. Debus, C.T. Hua, J.-F. Karczewski, H. Laplace, P. Levacher, Ph. Lognonné, C. Malique, M. Menvielle, G. Mouli, J.-P. Pommereau, K. Quotb, J. Runavot, D. Vienne, F. Grunthaner, F. Kuhnke, G. Musmann, R. Rieder, H. Wänke, T. Economou, M. Herring, A. Lane, and C.P. McKay. A sophisticated lander for scientific exploration of mars: scientific objectives and implementation of the mars-96 small station. *Planetary and Space Science*, 46(6-7):717–737, June 1998. doi: 10.1016/s0032-0633(98)00008-7. URL `https://doi.org/10.1016/s0032-0633(98)00008-7`.

P. Lognonné, V.N. Zharkov, J.F. Karczewski, B. Romanowicz, M. Menvielle, G. Poupinet, B. Brient, C. Cavoit, A. Desautez, B. Dole, D. Franqueville, J. Gagnepain-Beyneix, H. Richard, P. Schibler, and N. Striebig. The seismic OPTIMISM experiment. *Planetary and Space*

Science, 46(6-7):739–747, June 1998. doi: 10.1016/s0032-0633(98)00009-9. URL https://doi.org/10.1016/s0032-0633(98)00009-9.

P. Lognonné, W. B. Banerdt, D. Giardini, W. T. Pike, U. Christensen, P. Laudet, S. de Raucourt, P. Zweifel, S. Calcutt, M. Bierwirth, K. J. Hurst, F. Ijpelaan, J. W. Umland, R. Llorca-Cejudo, S. A. Larson, R. F. Garcia, S. Kedar, B. Knapmeyer-Endrun, D. Mimoun, A. Mocquet, M. P. Panning, R. C. Weber, A. Sylvestre-Baron, G. Pont, N. Verdier, L. Kerjean, L. J. Facto, V. Gharakanian, J. E. Feldman, T. L. Hoffman, D. B. Klein, K. Klein, N. P. Onufer, J. Paredes-Garcia, M. P. Petkov, J. R. Willis, S. E. Smrekar, M. Drilleau, T. Gabsi, T. Nebut, O. Robert, S. Tillier, C. Moreau, M. Parise, G. Aveni, S. Ben Charef, Y. Bennour, T. Camus, P. A. Dandonneau, C. Desfoux, B. Lecomte, O. Pot, P. Revuz, D. Mance, J. tenPierick, N. E. Bowles, C. Charalambous, A. K. Delahunty, J. Hurley, R. Irshad, Huafeng Liu, A. G. Mukherjee, I. M. Standley, A. E. Stott, J. Temple, T. Warren, M. Eberhardt, A. Kramer, W. Kühne, E.-P. Miettinen, M. Monecke, C. Aicardi, M. André, J. Baroukh, A. Borrien, A. Bouisset, P. Boutte, K. Brethomé, C. Brysbaert, T. Carlier, M. Deleuze, J. M. Desmarres, D. Dilhan, C. Doucet, D. Faye, N. Faye-Refalo, R. Gonzalez, C. Imbert, C. Larigauderie, E. Locatelli, L. Luno, J.-R. Meyer, F. Mialhe, J. M. Mouret, M. Nonon, Y. Pahn, A. Paillet, P. Pasquier, G. Perez, R. Perez, L. Perrin, B. Pouilloux, A. Rosak, I. Savin de Larclause, J. Sicre, M. Sodki, N. Toulemont, B. Vella, C. Yana, F. Alibay, O. M. Avalos, M. A. Balzer, P. Bhandari, E. Blanco, B. D. Bone, J. C. Bousman, P. Bruneau, F. J. Calef, R. J. Calvet, S. A. D'Agostino, G. de los Santos, R. G. Deen, R. W. Denise, J. Ervin, N. W. Ferraro, H. E. Gengl, F. Grinblat, D. Hernandez, M. Hetzel, M. E. Johnson, L. Khachikyan, J. Y. Lin, S. M. Madzunkov, S. L. Marshall, I. G. Mikellides, E. A. Miller, W. Raff, J. E. Singer, C. M. Sunday, J. F. Villalvazo, M. C. Wallace, D. Banfield, J. A. Rodriguez-Manfredi, C. T. Russell, A. Trebi-Ollennu, J. N. Maki, E. Beucler, M. Böse, C. Bonjour, J. L. Berenguer, S. Ceylan, J. Clinton, V. Conejero, I. Daubar, V. Dehant, P. Delage, F. Euchner, I. Estève, L. Fayon, L. Ferraioli, C. L. Johnson, J. Gagnepain-Beyneix, M. Golombek, A. Khan, T. Kawamura, B. Kenda, P. Labrot, N. Murdoch, C. Pardo, C. Perrin, L. Pou, A. Sauron, D. Savoie, S. Stähler, E. Stutzmann, N. A. Teanby, J. Tromp, M. van Driel, M. Wieczorek, R. Widmer-Schnidrig, and J. Wookey. SEIS: Insight's Seismic Experiment for Internal Structure of Mars. *Space Science Reviews*, 215(1), January 2019. ISSN 0038-6308, 1572-9672. doi: 10.1007/s11214-018-0574-6.

P. Lognonné, W. B. Banerdt, W. T. Pike, D. Giardini, U. Christensen, R. F. Garcia, T. Kawamura, S. Kedar, B. Knapmeyer-Endrun, L. Margerin, F. Nimmo, M. Panning, B. Tauzin, J.-R. Scholz, D. Antonangeli, S. Barkaoui, E. Beucler, F. Bissig, N. Brinkman, M. Calvet, S. Ceylan, C. Charalambous, P. Davis, M. van Driel, M. Drilleau, L. Fayon, R. Joshi, B. Kenda, A. Khan, M. Knapmeyer, V. Lekic, J. McClean, D. Mimoun, N. Murdoch, L. Pan, C. Perrin, B. Pinot, L. Pou, S. Menina, S. Rodriguez, C. Schmelzbach, N. Schmerr, D. Sollberger, A. Spiga, S. Stähler, A. Stott, E. Stutzmann, S. Tharimena, R. Widmer-Schnidrig, F. Andersson, V. Ansan, C. Beghein, M. Böse, E. Bozdag, J. Clinton, I. Daubar, P. Delage, N. Fuji, M. Golombek, M. Grott, A. Horleston, K. Hurst, J. Irving, A. Jacob, J. Knollenberg, S. Krasner, C. Krause, R. Lorenz, C. Michaut, R. Myhill, T. Nissen-Meyer, J. ten Pierick, A.-C. Plesa, C. Quantin-Nataf, J. Robertsson, L. Rochas, M. Schimmel, S. Smrekar, T. Spohn, N. Teanby, J. Tromp, J. Vallade, N. Verdier, C. Vrettos, R. Weber, D. Banfield, E. Barrett, M. Bierwirth, S. Calcutt, N. Compaire, C.L. Johnson, D. Mance, F. Euchner, L. Kerjean, G. Mainsant, A. Mocquet, J. A Rodriguez Manfredi, G. Pont, P. Laudet, T. Nebut, S. de Raucourt, O. Robert, C. T. Russell,

A. Sylvestre-Baron, S. Tillier, T. Warren, M. Wieczorek, C. Yana, and P. Zweifel. Constraints on the shallow elastic and anelastic structure of Mars from InSight seismic data. *Nature Geoscience*, February 2020. ISSN 1752-0894, 1752-0908. doi: 10.1038/s41561-020-0536-y.

J. N. Maki, M. Golombek, R. Deen, H. Abarca, C. Sorice, T. Goodsall, M. Schwochert, M. Lemmon, A. Trebi-Ollennu, and W. B. Banerdt. The Color Cameras on the InSight Lander. *Space Science Reviews*, 214(6), September 2018. ISSN 0038-6308, 1572-9672. doi: 10.1007/s11214-018-0536-z.

Michio Otsuka. Azimuth and slowness anomalies of seismic waves measured on the central California seismographic array. Part I. Observations. *Bulletin of the Seismological Society of America*, 56(1):223–239, 02 1966. ISSN 0037-1106.

T. J. Parker, M. P. Golombek, F. J. Calef, N. R. Williams, S. LeMaistre, W. Folkner, I. J. Daubar, D. Kipp, E. Sklyanskiy, H. Lethcoe-Wilson, and R. Hausmann. Localization of the InSight Lander. In *Lunar and Planetary Science Conference*, Lunar and Planetary Science Conference, page 1948, Mar 2019.

D. Savoie, A. Richard, M. Goutaudier, N. P. Onufer, M. C. Wallace, D. Mimoun, K. Hurst, N. Verdier, P. Lognonné, and J. N. Maki. Determining True North on Mars by Using a Sundial on InSight. *Space Sci. Rev.*, 215:2, Jan 2019.

M. Schimmel, E. Stutzmann, F. Ardhuin, and J. Gallart. Polarized Earth's ambient microseismic noise. *Geochemistry, Geophysics, Geosystems*, 12(7), July 2011. ISSN 15252027. doi: 10.1029/2011GC003661.

T. A. Sullivan. Catalog of Apollo experiment operations. Technical report, Jan 1994.

Figure5.

InSight

SEIS

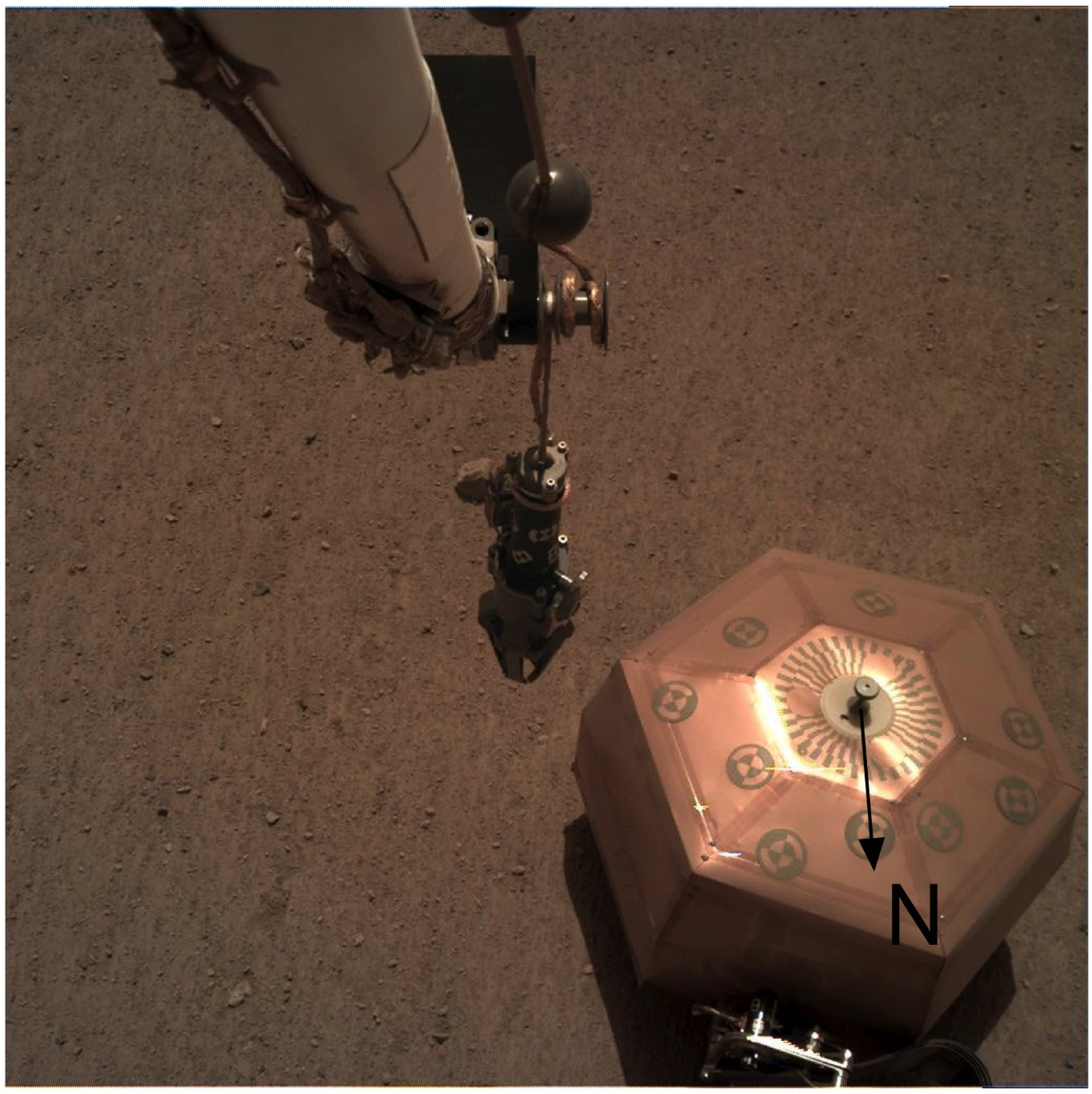

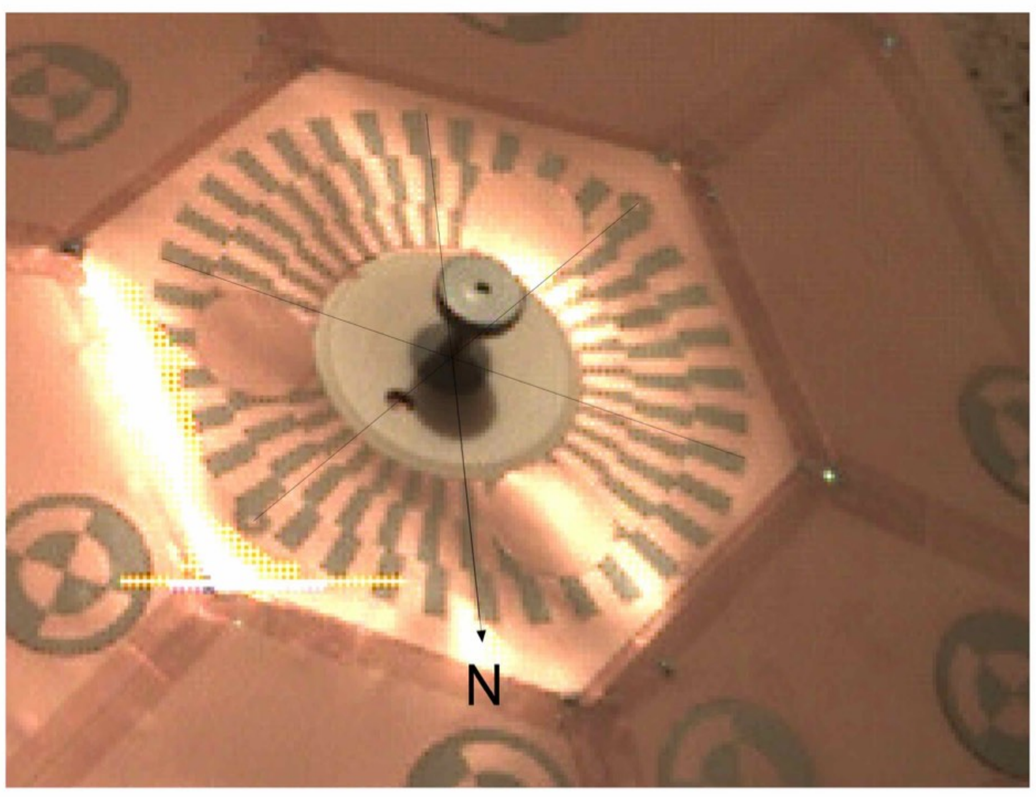

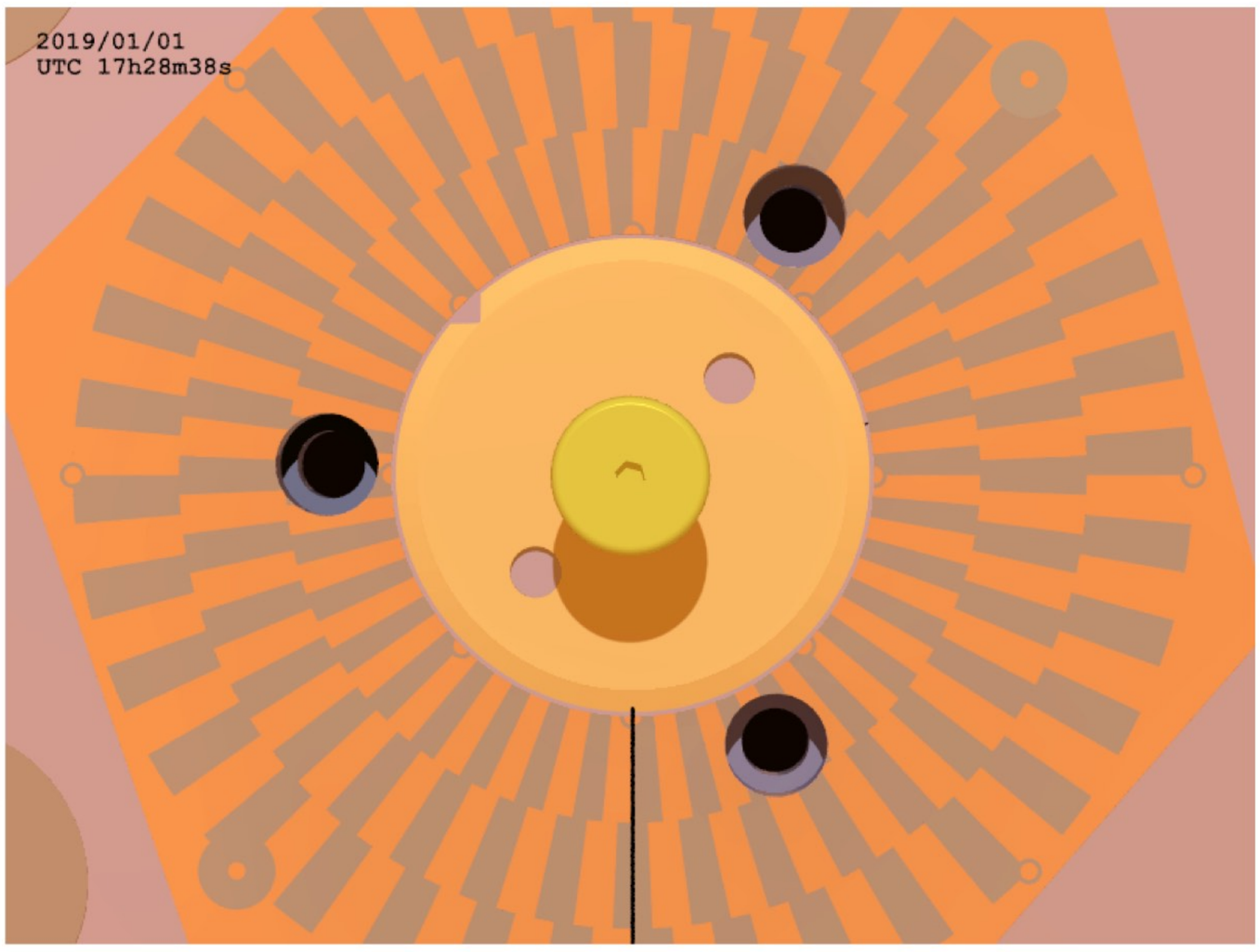

UTC = 17h28m38s
LMST = 12h49m37s
LTST= 12h00m24s
H = 0.0992°
α = 319.6436°
δ = -16.9434°
A = 0.2589°
h = 68.4926°
shadow =19.8 mm

sol 35 1/01/2019

Figure6.

InSight

SEIS

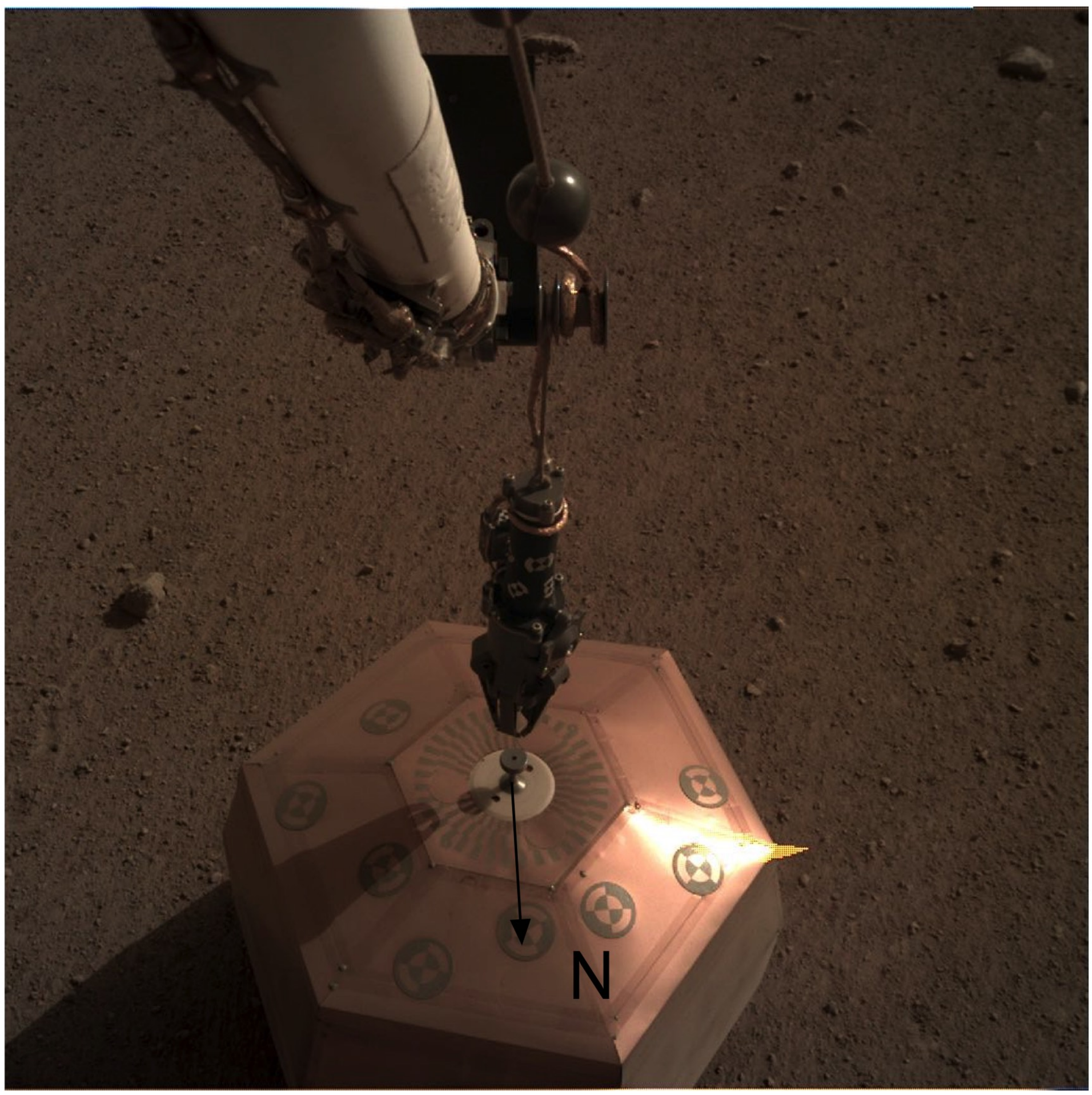

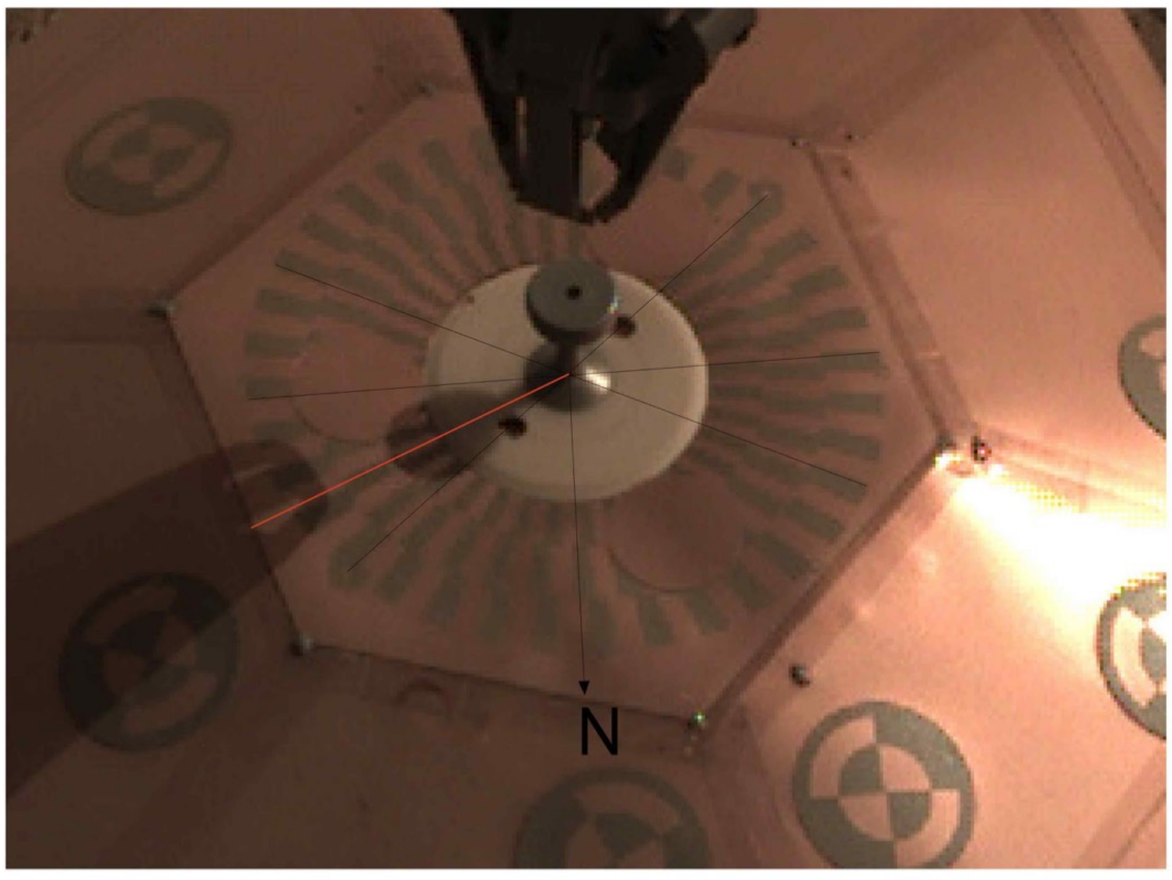

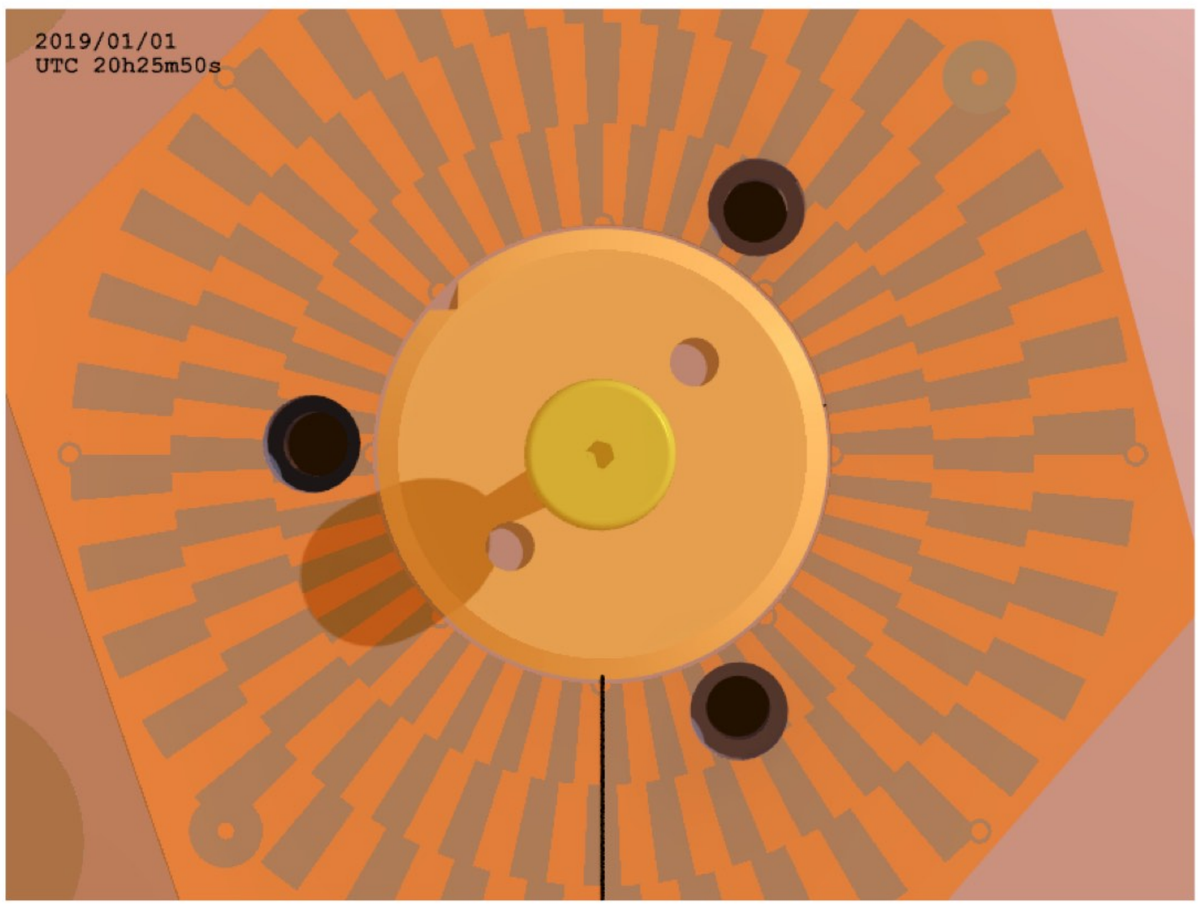

UTC = 20h25m50.0s
LMST = 15h42m05s
LTST = 14h52m50s
H = 43.2094°
α = 319.7126°
δ = -16.9204°
A = 62.1830°
h = 42.2166°
shadow = 39.9 mm

sol 35 1/01/2019

Figure9.

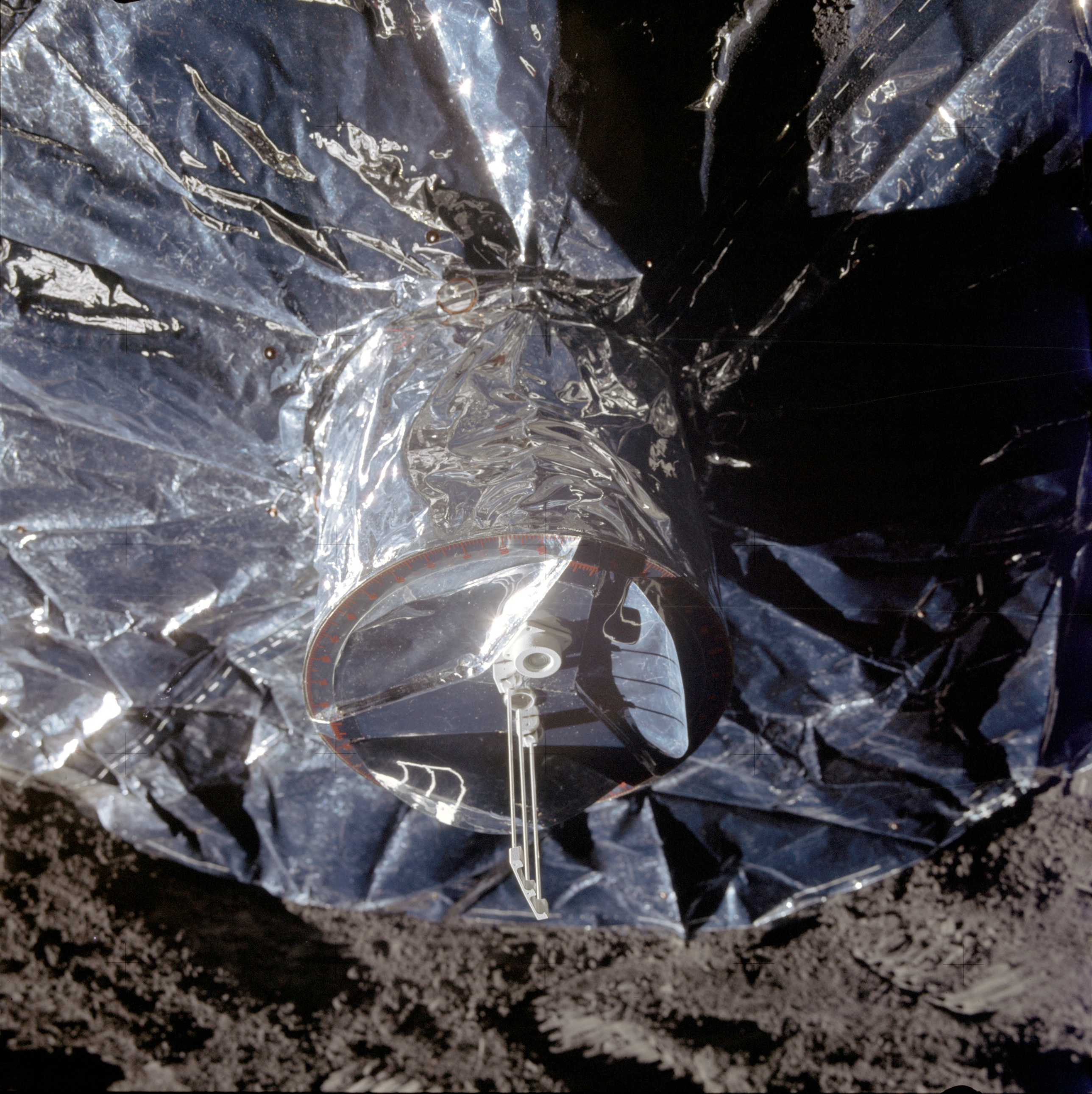

Figure3.

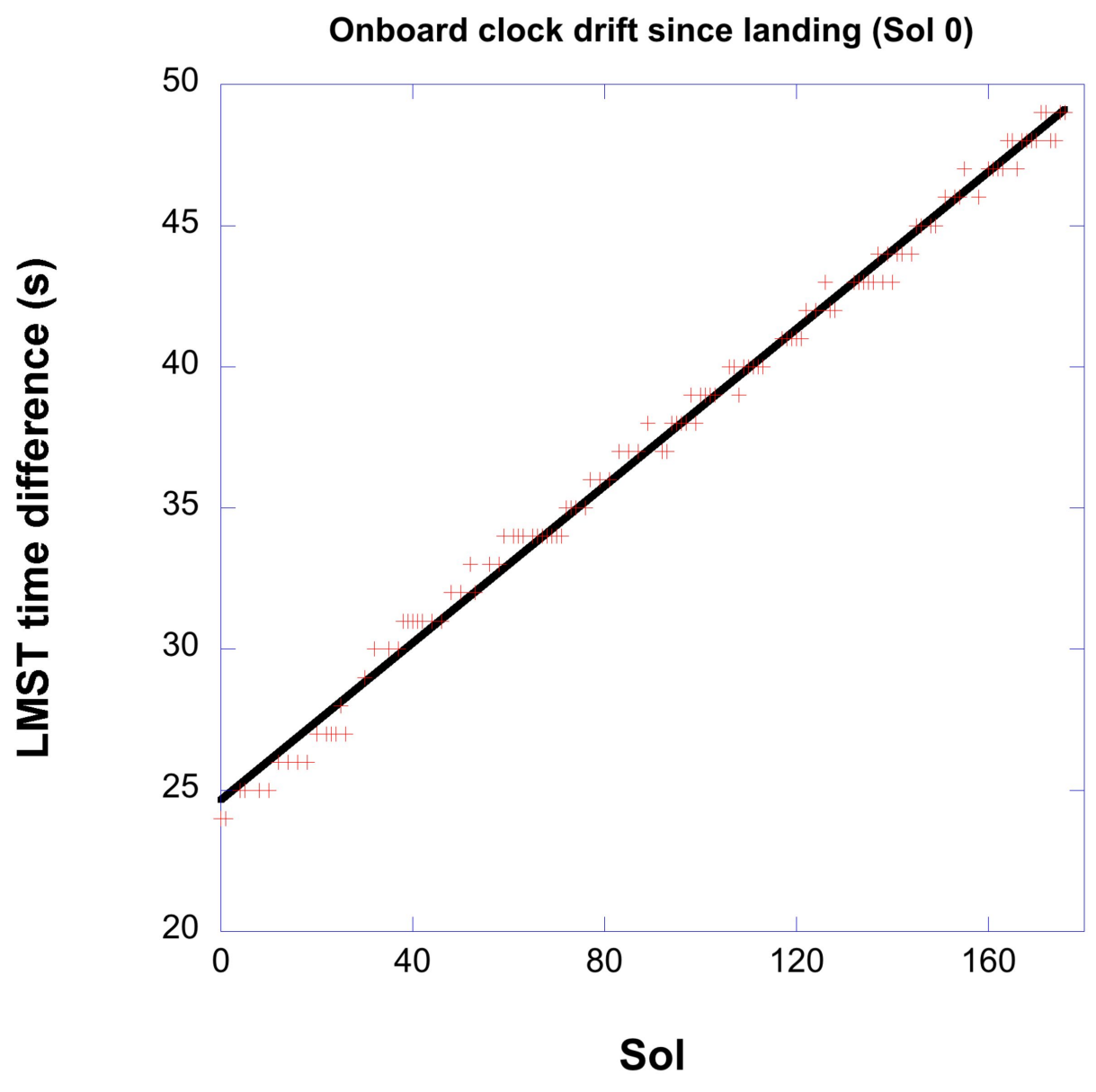
Onboard clock drift since landing (Sol 0)
LMST time difference (s)
50
45
40
35
30
25
20
0
40
80
120
160
Sol

Figure1a.

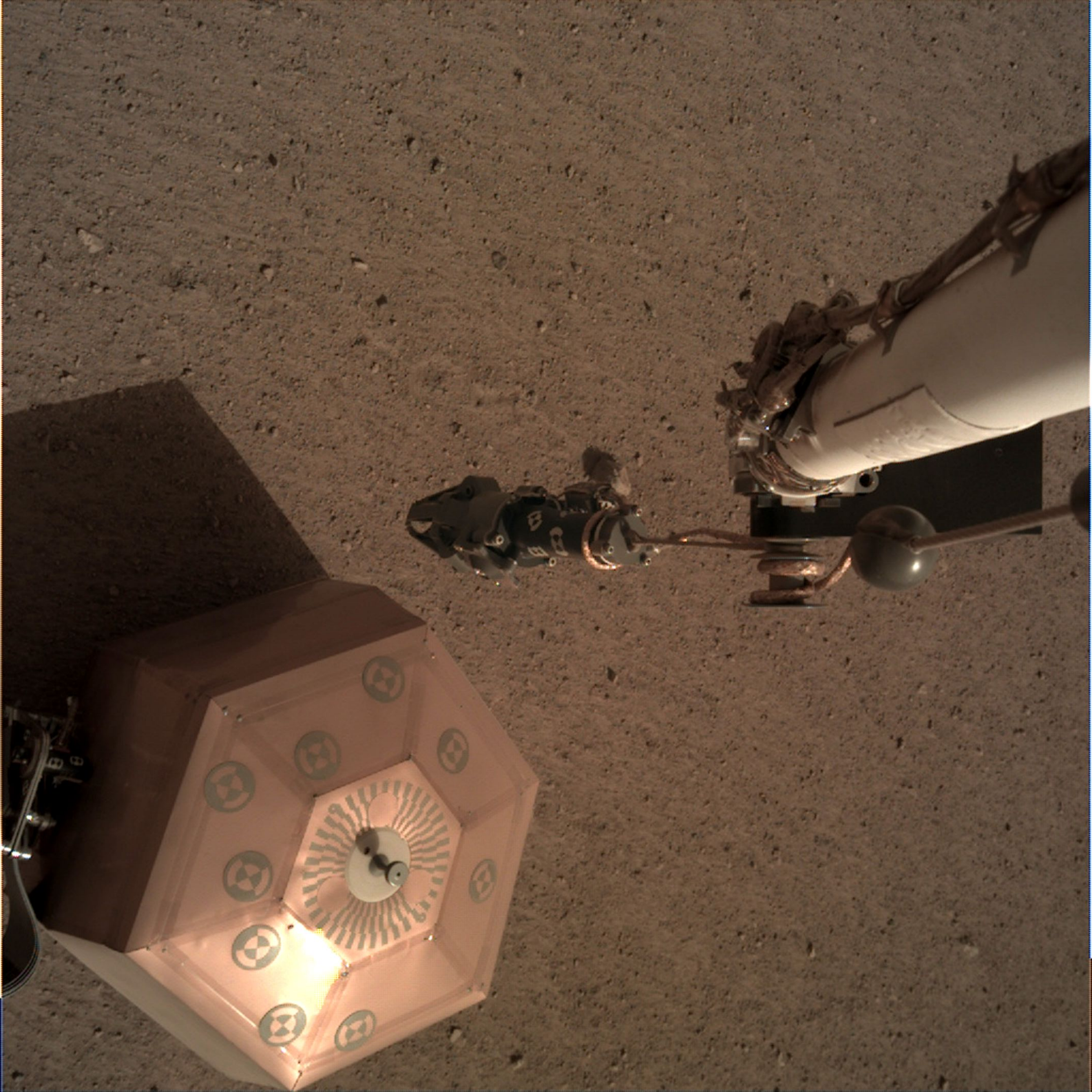

Figure1b.

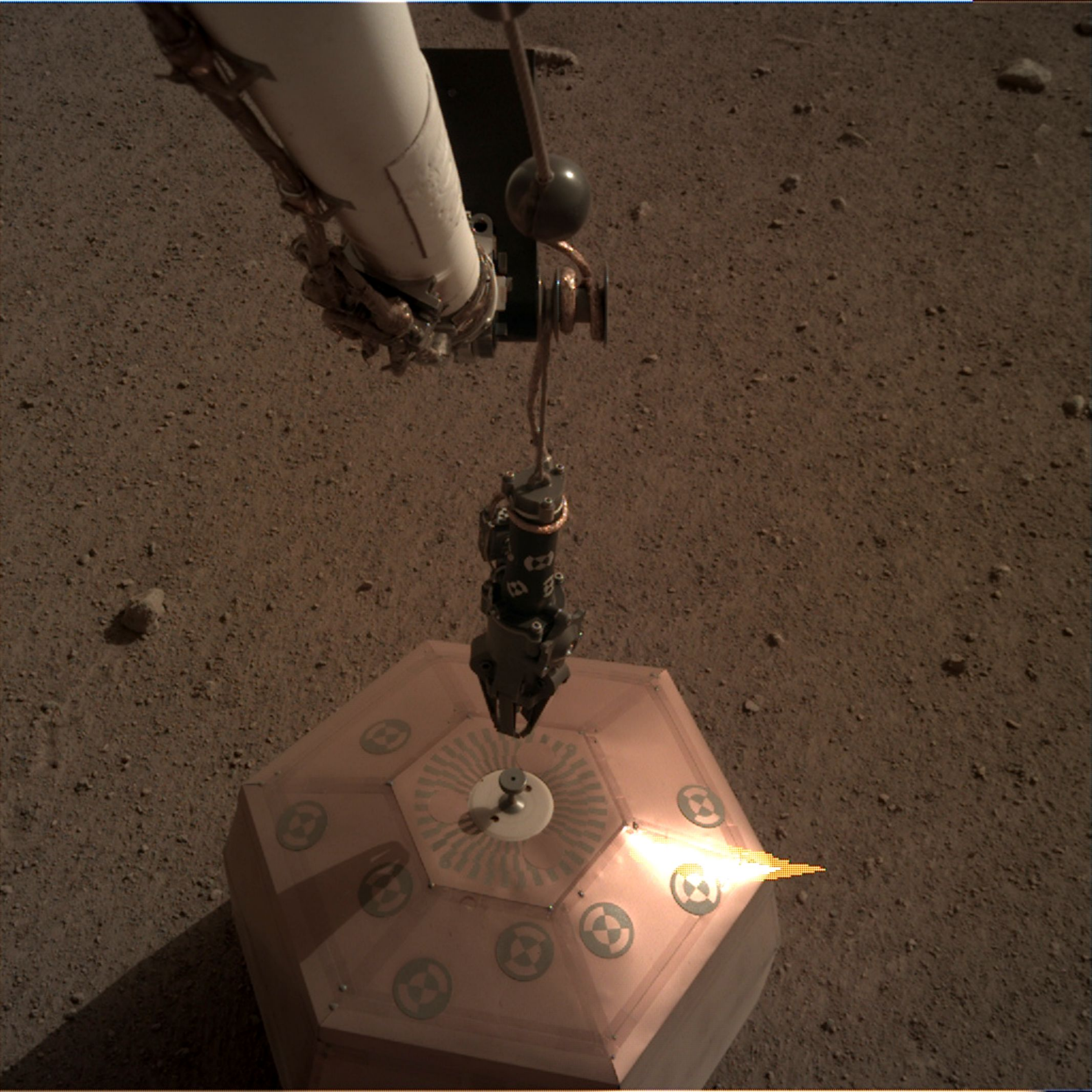

Figure4.

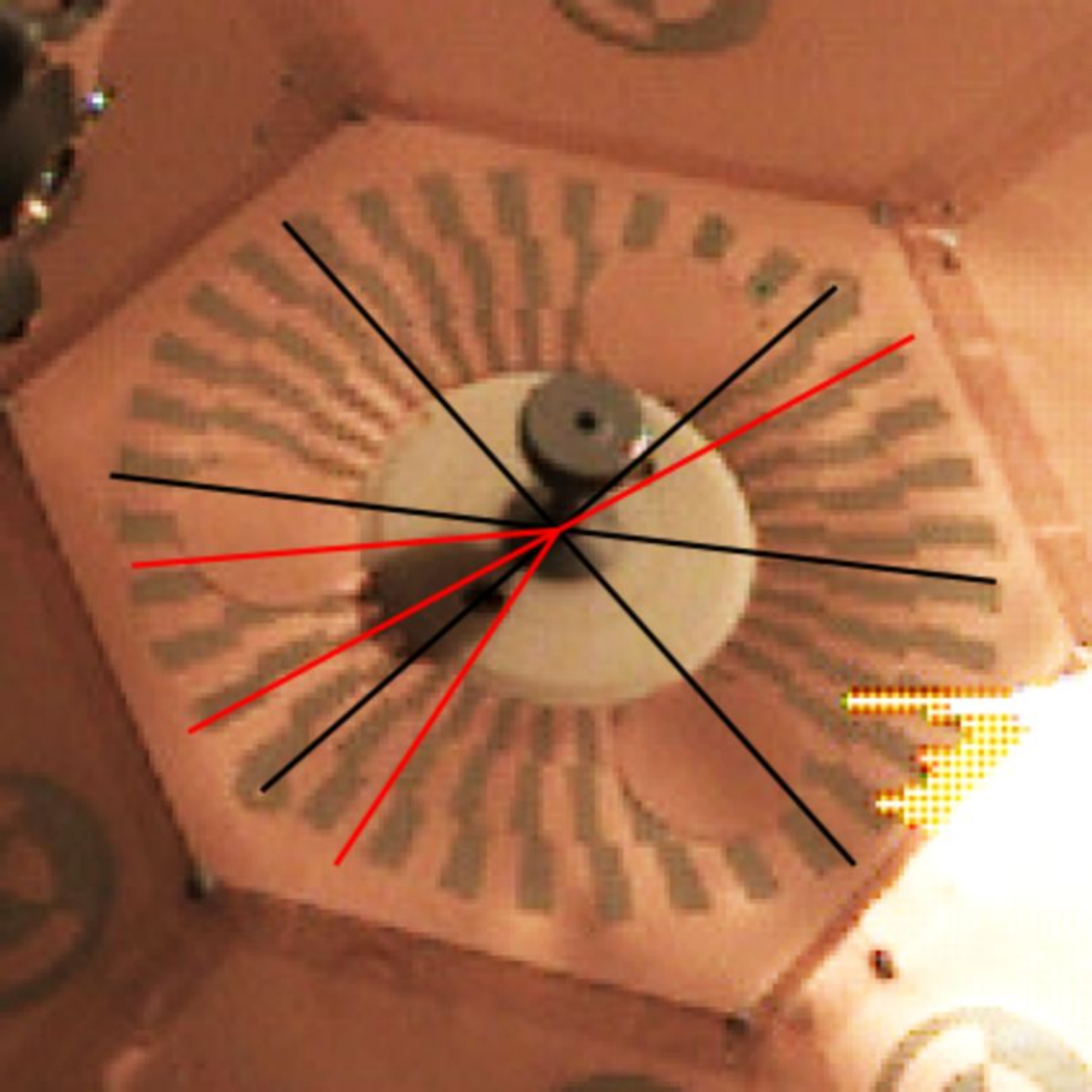

Figure2.

Camera
D for IDC (arm)
C for ICC (belly)

Sol number

Spacecraft clock time
Counting up in seconds

Color flag
F = color interpolated
_ = raw, not interpolated

Sequence ID

D001R0010_597419012EDR_F0004_0010M_.PNG

Stereo pair information (counter and eye)
000M = mono image
001L, 001R = matched left and right eyes (images taken on the same sol having the same number are a matched pair)

Mesh (digital elevation model) ID
00 = not part of a mesh
10-63: part of a mesh that will match across the entire mission
00-09: part of a mesh used only within the same sol

Mosaic ID
00 = not part of any mosaic
10-63: part of a mosaic that will match across the entire mission
00-09: part of a mosaic that will match only within the same sol

NASA / JPL-Caltech / Emily Lakdawalla

Figure8.

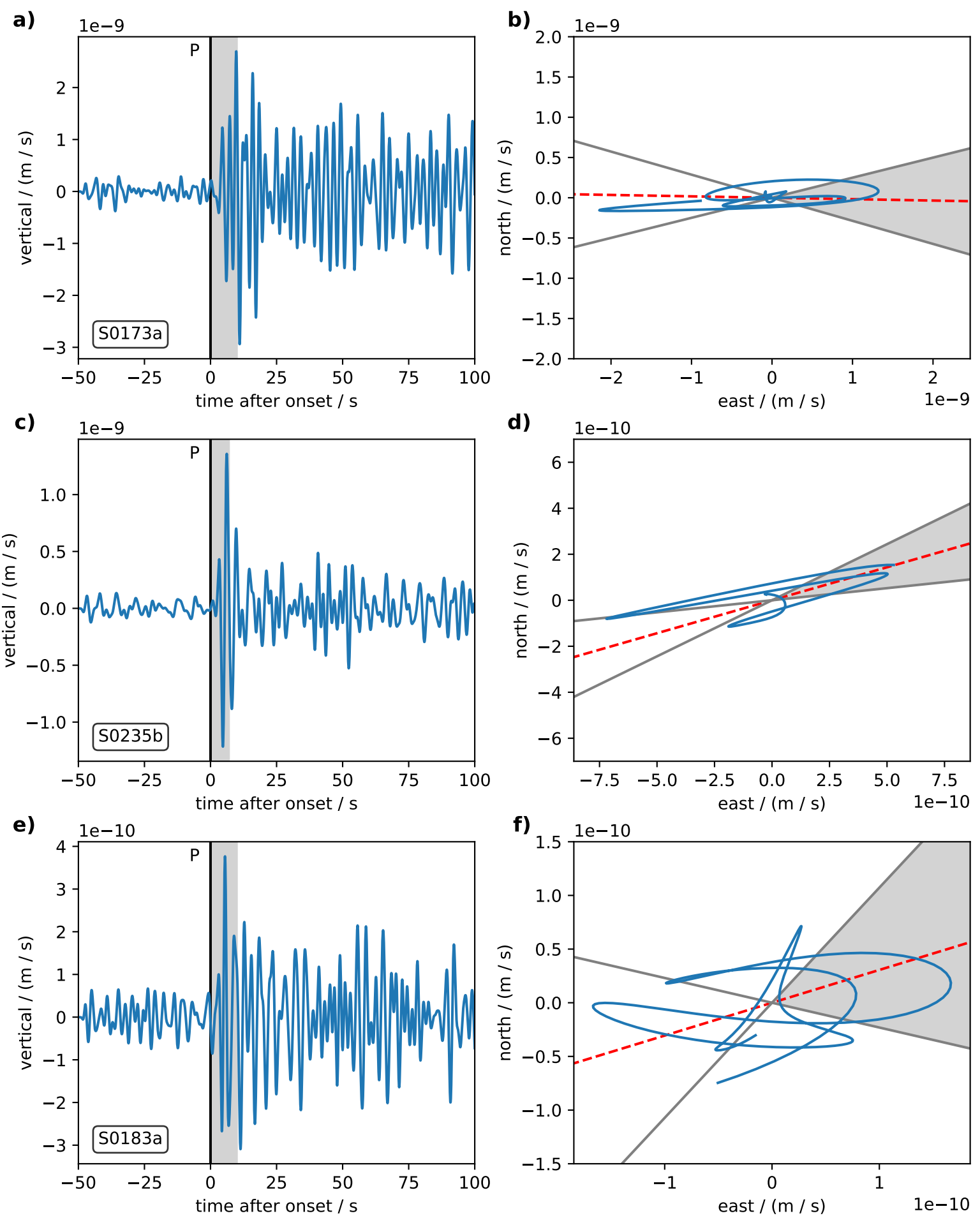
a)
1e−9
P
vertical / (m / s)
S0173a
time after onset / s
b)
1e−9
north / (m / s)
east / (m / s)
1e−9
c)
1e−9
P
vertical / (m / s)
S0235b
time after onset / s
d)
1e−10
north / (m / s)
east / (m / s)
1e−10
e)
1e−10
P
vertical / (m / s)
S0183a
time after onset / s
f)
1e−10
north / (m / s)
east / (m / s)
1e−10

Figure7.

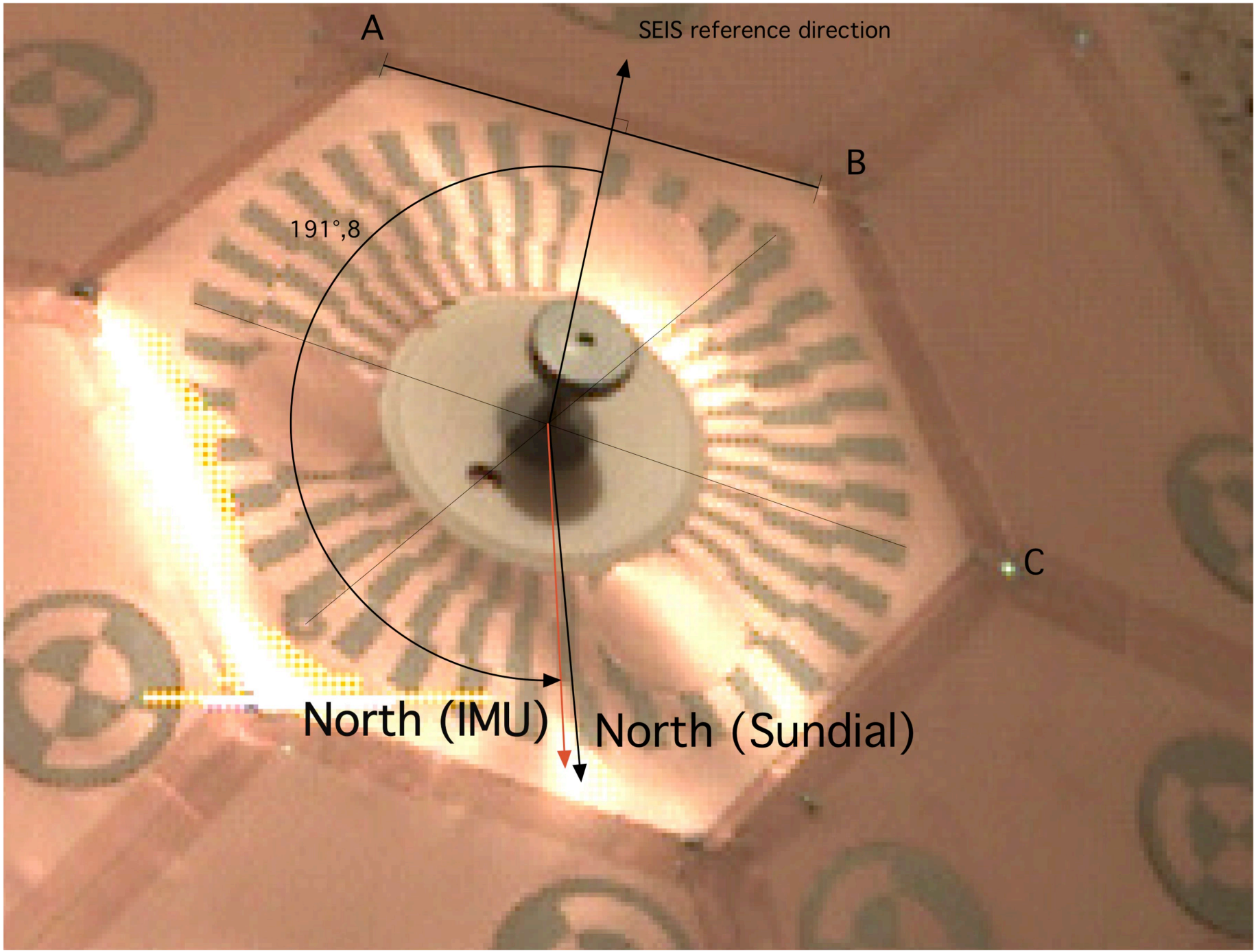
A
SEIS reference direction
B
191°,8
C
North (IMU)
North (Sundial)